Journal of Asian Earth Sciences 114 (2015) 299–304

Contents lists available at ScienceDirect

Journal of Asian Earth Sciences

journal homepage: www.elsevier.com/locate/jseaes

Statistical analysis of earthquakes after the 1999 M_W 7.7 Chi-Chi, Taiwan, earthquake based on a modified Reasenberg–Jones model

Yuh-Ing Chen [a,*], Chi-Shen Huang [b], Jann-Yenq Liu [b]

[a] Institute of Statistics, National Central University, Chung-Li, Taiwan
[b] Institute of Space Science, National Central University, Chung-Li, Taiwan

ARTICLE INFO

Article history:
Received 26 June 2014
Received in revised form 4 February 2015
Accepted 13 February 2015
Available online 9 March 2015

Keywords:
Chi-Chi earthquake
Gutenberg–Richter law
Reasenberg–Jones model
Receiver operating characteristic curve
Relative hazard map
Utsu–Omori law
Youden index

ABSTRACT

We investigated the temporal–spatial hazard of the earthquakes after the 1999 September 21 M_W = 7.7 Chi-Chi shock in a continental region of Taiwan. The Reasenberg–Jones (RJ) model (Reasenberg and Jones, 1989, 1994) that combines the frequency-magnitude distribution (Gutenberg and Richter, 1944) and time-decaying occurrence rate (Utsu et al., 1995) is conventionally employed for assessing the earthquake hazard after a large shock. However, it is found that the b values in the frequency-magnitude distribution of the earthquakes in the study region dramatically decreased from background values after the Chi-Chi shock, and then gradually increased up. The observation of a time-dependent frequency-magnitude distribution motivated us to propose a modified RJ model (MRJ) to assess the earthquake hazard. To see how the models perform on assessing short-term earthquake hazard, the RJ and MRJ models were separately used to sequentially forecast earthquakes in the study region. To depict the potential rupture area for future earthquakes, we further constructed relative hazard (RH) maps based on the two models. The Receiver Operating Characteristics (ROC) curves (Swets, 1988) finally demonstrated that the RH map based on the MRJ model was, in general, superior to the one based on the original RJ model for exploring the spatial hazard of earthquakes in a short time after the Chi-Chi shock.

1. Introduction

Large earthquakes followed by devastating shocks usually pose a significant hazard to populated areas. The information about the near real time earthquake hazard would then be necessary for decision makers to determine optimal treatments of damaged structures. Therefore, it is often of great importance to evaluate if any large earthquakes are likely to occur in the short period that follows, especially, a drastic shock. To answer the question, many authors have discussed how to evaluate the earthquake hazard with respect to their magnitudes and occurrence time. For example, Gutenberg and Richter (1944) proposed the frequency-magnitude distribution of earthquakes, known as the Gutenberg–Richter law, as given by

$$\log_{10} N(M) = a - bM, \quad \text{for } M > M_c, \tag{1}$$

where $N(M)$ is the number of earthquakes with magnitude larger or equal to M, b measures the ratio of small to large earthquakes, a is a constant related to the activity and M_c is the cut-off magnitude. In fact, the Gutenberg–Richter law implies that the distribution of earthquake magnitudes is an exponential distribution left-truncated at M_c. Therefore, for $M > M_c$, the associate survival function or probability of having an earthquake with magnitude larger or equal to M is

$$S(M) = P\ (\text{Event with magnitude} > M) = \exp\{-\beta(M - M_c)\}, \tag{2}$$

where $\beta = b\ ln\ 10$. Note that the b value, as one of the most important parameters in seismology, has been observed to vary temporally and spatially (Utsu, 1971; Smith, 1981; Wiemer and Wyss, 1997; Wiemer and Katsumata, 1999).

On the other hand, the time-decaying occurrence rate of an aftershock sequence after its mainshock is usually described by the Utsu–Omori power law (Utsu et al., 1995)

$$\lambda(t) = K/(t + c)^p \quad \text{for } t > t_0, \tag{3}$$

where $\lambda(t)$ is the number of events per unit time at time t after the mainshock, K depends on the total number of aftershocks in the sequence, c is related to the activity in the earliest stage of the sequence, and the most important parameter p is the decay parameter. The maximum likelihood estimation of the related parameters was thoroughly discussed in Ogata (1983). Recent studies show that the p value is not only different for a variety of aftershock sequences, but also varies spatially in the rupture area of a

* Corresponding author.

http://dx.doi.org/10.1016/j.jseaes.2015.02.018
1367-9120/

sequence of aftershocks (Kisslinger and Jones, 1991; Utsu et al., 1995; Wiemer and Katsumata, 1999).

Assuming that the magnitude and occurrence time of earthquakes are independent, Reasenberg and Jones (1989, 1994) combined the Gutenberg–Richter law and the Utsu–Omori power law to describe the time-magnitude distribution of aftershocks, usually referred to as the RJ model. Based on the RJ model, the number of events with magnitude equal to or larger than M per unit time at time t after the mainshock is then given by

$$\lambda(t,M) = \lambda(t)S(M) \text{ for } t > t_0 \text{ and } M > M_c, \tag{4}$$

where $S(M)$ and $\lambda(t)$ are specified in (2) and (3), respectively. The probability of one or more earthquakes with magnitude greater than M occurring in the time rage (T_1, T_2), $T_1 > t_0$, is finally evaluated as

$$P = 1 - \exp\left\{-S(M)\int_{T_1}^{T_2}\lambda(t)dt\right\}. \tag{5}$$

For spatial mapping of aftershock hazard, Wiemer (2000) further obtained the probabilistic aftershock hazard (PAH) map by computing the value of P (5) in each of the dense gridpoints over a possible rupture area. The PAH map then provides some information about the possible rupture area of future earthquakes.

It was recognized, however, that the magnitude distribution could depend explicitly on time (Vere-Jones, 1992). In fact, the b value was shown to be a function of time for the 1999 October 16 M_W 7.1 Hector Mine aftershock sequence (Wiemer et al., 2002). Moreover, it is usually believed that aftershocks of larger magnitude are more likely to occur right after the mainshock, but are less likely to occur as time goes by. Therefore, earthquakes following a large shock within a short time period would preserve a time-dependent frequency-magnitude distribution, which motivates a modification of the original Gutenberg–Richter law and hence the RJ model.

In this study, we modify the RJ model by incorporating a simple linear time-trend for the β value in (2) to describe the hazard of earthquakes that occurred in a short time after the M_W 7.7 Chi-Chi shock with epicenter (23.85°N, 120.82°E) that occurred at 0147 LT, 21 September 1999 in Taiwan. We then employ the modified RJ or MRJ models to make a sequential evaluation of earthquake hazard after the Chi-Chi shock in a region that covers Chi-Chi's epicenter. We further construct a relative hazard (RH) map based on the MRJ or RJ model for identifying the possible rupture area of future earthquakes after the Chi-Chi shock. Finally, the area under the Receiver Operating Characteristics (ROC) curve (Swets, 1988), called AUC, and the Youden index (Youden, 1950) are used to assess the performance of the RH map on alarming future earthquakes.

2. Statistical model

Suppose that the β value in (2) is a function of time t, namely, $\beta(t)$. Then, the associated conditional survivor function of magnitude M at time t is

$$\begin{aligned} S(M|t) &= P(\text{Event with magnitude} > M \text{ at time } t) \\ &= \exp\{-\beta(t)(M - M_c)\} \text{ for } t > 0 \text{ and } M > M_c. \end{aligned} \tag{6}$$

In this paper, we consider $\beta(t) = \alpha_0 + \alpha_1 ln\ t$. Therefore, the original RJ model can be modified to yield the MRJ model with

$$\lambda(t,M) = \lambda(t)S(M|t) \text{ for } t > t_0 \text{ and } M > M_c. \tag{7}$$

To evaluate the earthquake hazard based on the proposed MRJ model, we can find the expected number of earthquakes with magnitude greater than M occurring in the time range (T_1, T_2) after the mainshock, $\int_{T_1}^{T_2}\lambda(t)S(M|t)dt$, or compute the probability of having one or more such earthquakes as

$$P = 1 - \exp\left\{-\int_{T_1}^{T_2}\lambda(t)S(M|t)dt\right\}. \tag{8}$$

When observing the events with magnitude M_i occurring at time t_i, $i = 1, \ldots, N$, the likelihood function of parameter $\boldsymbol{\theta} = (K, c, p, \alpha_0, \alpha_1)$ is given by:

$$L(\boldsymbol{\theta}) = \prod_{i=1}^{N}\lambda(t_i)\exp\left\{-\int_{t_{i-1}}^{t_i}\lambda(s)ds\right\}\prod_{i=1}^{N}\beta(t_i)\exp\{-\beta(t_i)(M_i - M_c)\}.$$

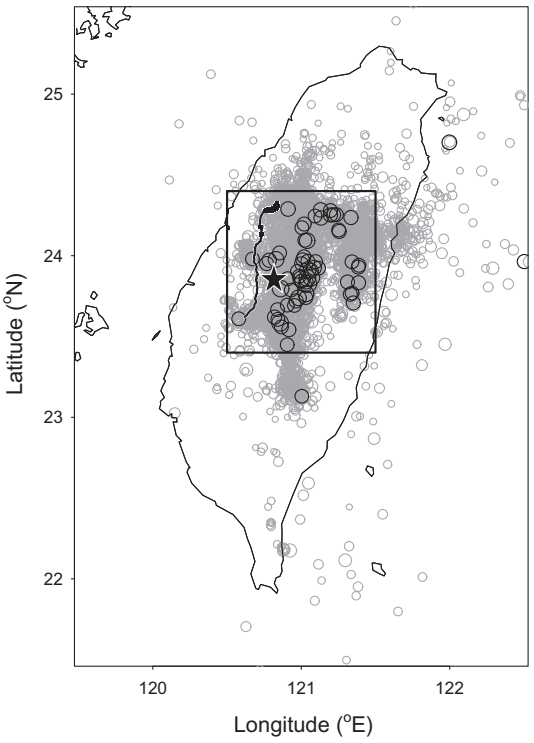

Fig. 1. Earthquakes following the 1999 September 21 M_W = 7.7 Chi-Chi shock near the Chelongpu fault in Taiwan. The Chelongpu fault is depicted by the black line and the black star locates the epicenter of the Chi-Chi earthquake. The gray and black circles in the rectangular region under study represent $M \geqslant 2.6$ and $M \geqslant 5.0$ earthquakes, respectively, that occurred within 20 days after the Chi-Chi earthquake.

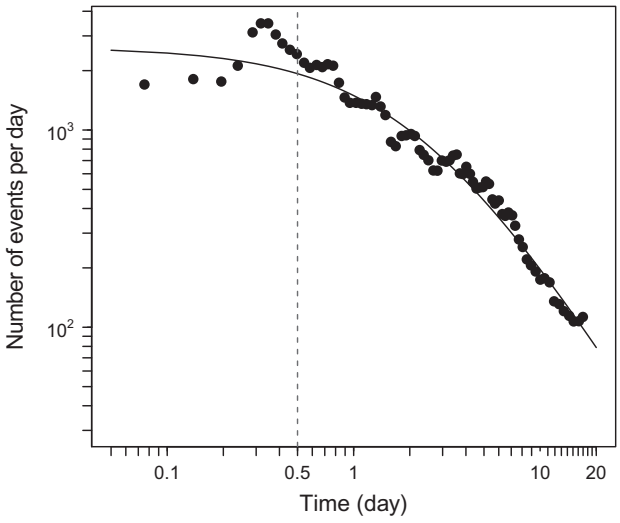

Fig. 2. The occurrence rate of earthquakes after the Chi-Chi shock.

The associated log-likelihood function is then obtained as

$$\begin{aligned} ln\ L(\boldsymbol{\theta}) &= \sum_{i=1}^{N} ln\ \lambda(t_i) - \int_0^{t_N} \lambda(s)ds \\ &\quad + \sum_{i=1}^{N} \{ln(\alpha_0 + \alpha_1 ln\ t_i) - (\alpha_0 + \alpha_1 ln\ t_i)(M_i - M_c)\} \\ &= N\ ln\ K - p\sum_{i=1}^{N} ln(t_i + c) - K \cdot A(c,p) \\ &\quad + \sum_{i=1}^{N} \{ln(\alpha_0 + \alpha_1 ln\ t_i) - (\alpha_0 + \alpha_1 ln\ t_i)(M_i - M_c)\}, \end{aligned}$$

where

$$A(c,p) = \begin{cases} \frac{\{(t_N+c)^{1-p} - c^{1-p}\}}{(1-p)}, & p \neq 1 \\ ln(t_N + c) - ln\ c, & p = 1. \end{cases}$$

Note that the maximum likelihood estimator (MLE) of $\boldsymbol{\theta}$, denoted by $\hat{\boldsymbol{\theta}} = (\widehat{K},\ \hat{c}, \hat{p},\ \hat{\alpha}_0,\ \hat{\alpha}_1)$, is the value of $\boldsymbol{\theta}$ such that $L(\boldsymbol{\theta})$ or $\ln L(\boldsymbol{\theta})$ reaches its maximum. The MLEs of $\lambda(t)$ and $S(M|t)$ are then given by

$$\hat{\lambda}(t) = \widehat{K}/(t + \hat{c})^{\hat{p}} \text{ for } t > t_0,$$

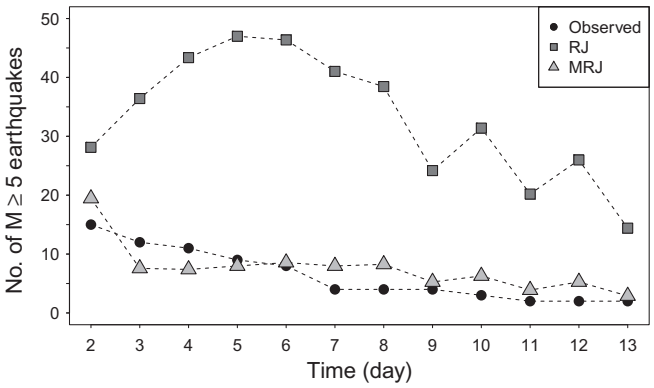

Fig. 5. The number of $M \geqslant 5.0$ earthquakes in the following 7 days. The black dots are the observed number of earthquakes in the following week. The squares and triangles denote the forecasted numbers of next-week earthquakes based on the RJ and MRJ models, respectively.

and

$$\widehat{S}(M|t) = \exp\{-(\hat{a}_0 + \hat{a}_1\ ln\ t)(M - M_c)\} \text{ for } M \geqslant M_c,$$

respectively. Hence, we forecast the number of earthquakes during (T_1, T_2) as

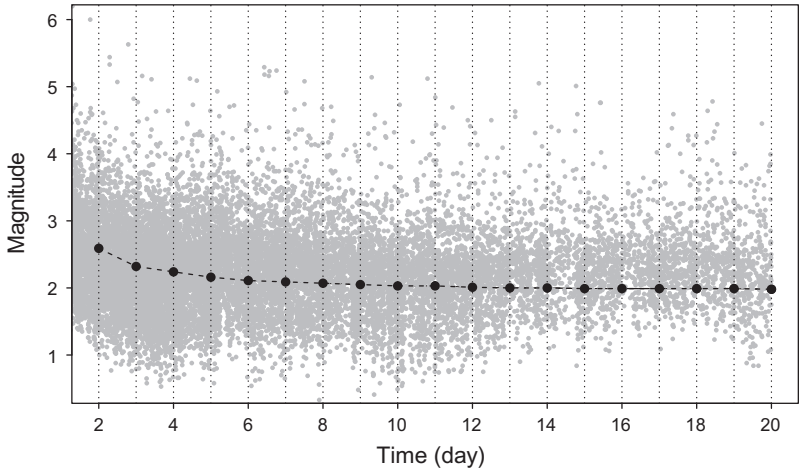

Fig. 3. The minimum magnitude for the complete recording of the cumulated earthquakes after the Chi-Chi shock. The gray dots on the background are the magnitudes of recorded earthquakes.

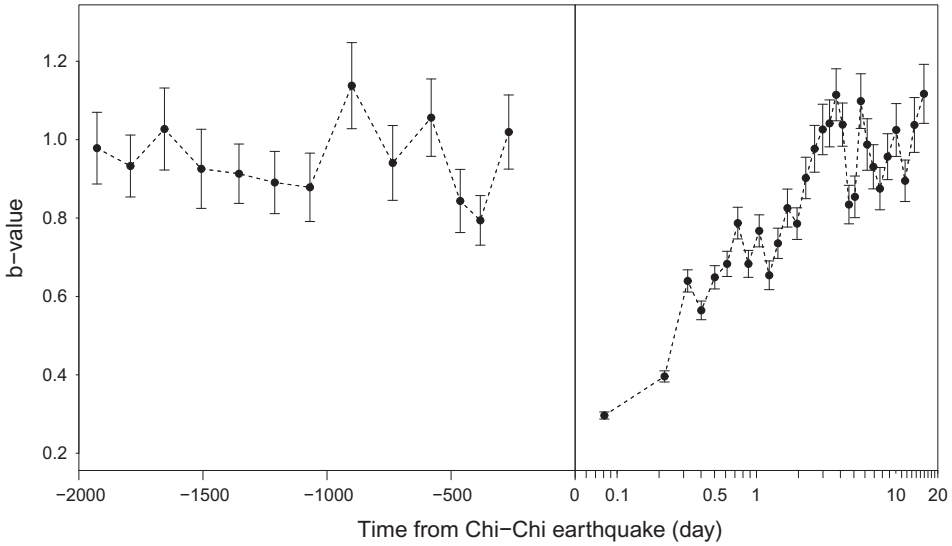

Fig. 4. The time-varying b values and the associated standard error for the earthquakes before and after the Chi-Chi shock.

$$n_M = \int_{T_1}^{T_2} \hat{\lambda}(t)\widehat{S}(M|t)dt, \tag{9}$$

and estimate the probability P (8) to be

$$\widehat{P} = 1 - \exp\left\{-\int_{T_1}^{T_2} \hat{\lambda}(t)\widehat{S}(M|t)dt\right\}. \tag{10}$$

3. Data analysis

In this paper, we analyze the earthquakes that occurred within 20 days after the Chi-Chi shock in the region of (23.4°N, 24.4°N) × (120.5°E, 121.5°E), as shown in Fig. 1. The earthquake catalog, including 21,569 events in total, being processed by 3-D relocation, was obtained from the Central Weather Bureau of Taiwan. The departure of the observed rates or numbers of events per day from the fitted curve (Fig. 2) indicates that the occurrence of the earthquakes in the first half day may not follow the Utsu–Omori's power law so well. Therefore, we take $t_0 = 0.5$ in Eq. (3) for the data analysis. The minimum magnitudes, M_c, for the complete recording of earthquakes (Wiemer and Wyss, 2000) till a certain number of days after the Chi-Chi shock are shown in Fig. 3. The minimum magnitudes apparently decrease with time, but are all less than 2.6. Therefore, based on the earthquakes with magnitudes greater than $M_c = 2.6$, we obtain the MLE of β in (2) along

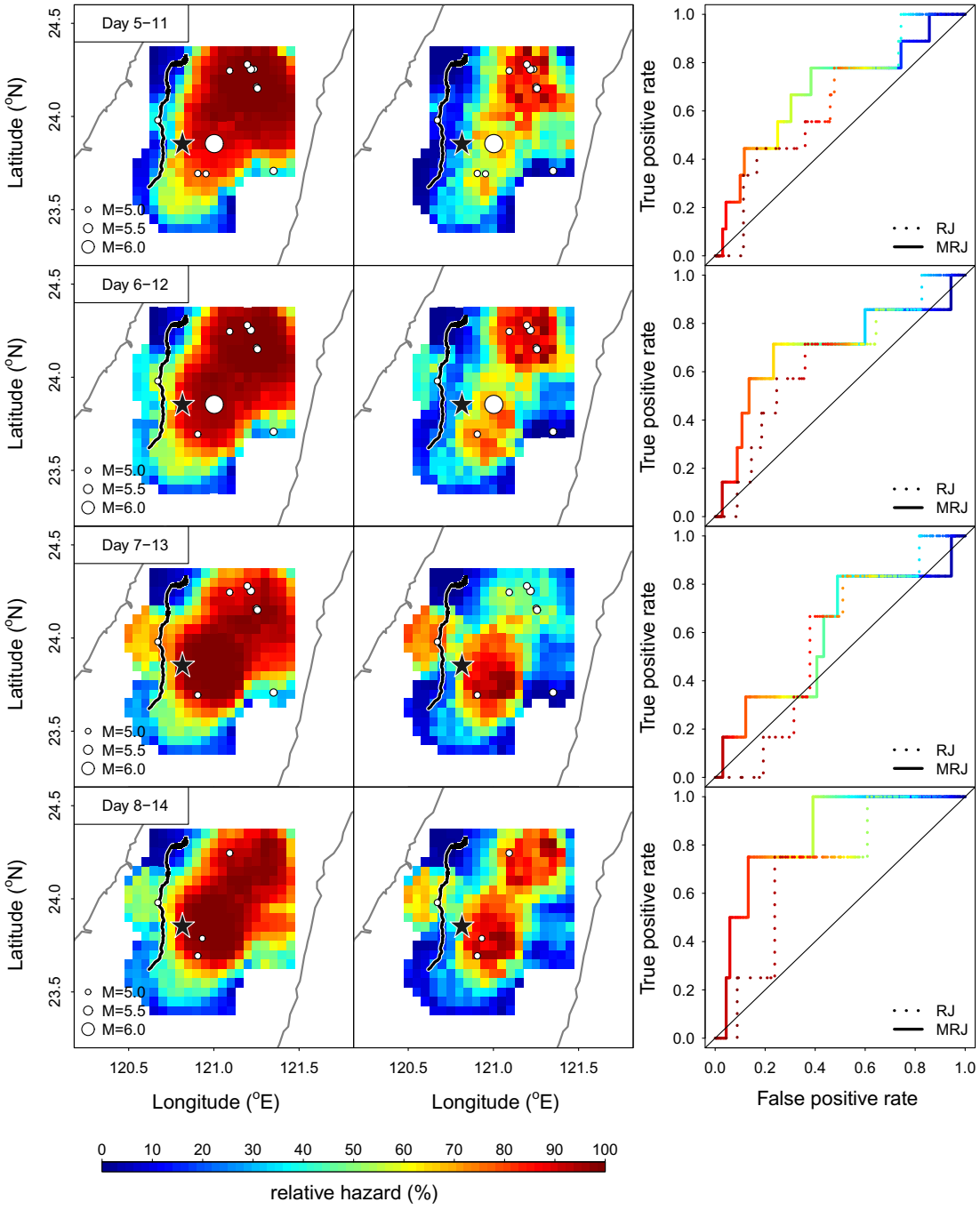

Fig. 6. The relative hazard maps constructed based on RJ (left) and MRJ (middle) models and the associated ROC curves (right). The relative hazards are computed on day n ($4 \leqslant n \leqslant 7$) after the Chi-Chi shock based on the completely recorded earthquakes. The star locates the epicenter of the Chi-Chi earthquake, the black line depicts the Chelongpu fault, and the white dots are the epicenters of the $M \geqslant 5.0$ earthquakes that occurred in the following 7 days (between $n+1$ and $n+7$ days) after the Chi-Chi shock.

with its standard error (Aki, 1965; Shi and Bolt, 1982) for each of the 250 events under study. The results, in Fig. 4, suggest a time-dependent b value with $\beta(t) = \alpha_0 + \alpha_1 \ln t$ as indicated in the MRJ model. Note that the b values of every 100 events in the study region before the Chi-Chi shock are also presented in Fig. 4 as the background b values, which are about 1. It was observed that the b values of the earthquakes after the Chi-Chi shock decrease dramatically from the background b values.

To employ the RJ or MRJ model for evaluating the short-term hazard of earthquakes in the study region, we sequentially fitted the model based on the completely recorded events within 0.5 and n days after the Chi-Chi shock for $2 \leqslant n \leqslant 13$. The number of $M \geqslant 5.0$ earthquakes between $n+1$ and $n+7$ days following the Chi-Chi shock in the study region is then forecasted according to the estimated RJ or MRJ model. Finally, the observed number of $M \geqslant 5.0$ earthquakes in the following 7 days and the forecasted ones based on RJ and MRJ models, respectively, are all presented in Fig. 5.

We demonstrate how to use the RJ or MRJ model for portraying the earthquake hazard over the study region in a short time after the Chi-Chi shock. To determine the minimum magnitude for the earthquakes that occurred between 0.5 and n days for $n = 4, 5, 6, 7$ after the Chi-Chi shock, we investigate the spatial variation of M_c in the study region based on dense grids centered at nodes separated by 0.05° with a radius of 0.2°. The value of M_c is computed at each gridpoint with at least 100 events, and the largest M_c is selected as the cut-off magnitude for all gridpoints which are 2.74, 2.72, 2.70, 2.66 for $n = 4, 5, 6, 7$, respectively. To assess the spatial hazard of earthquakes, we further consider a partition of the study region by using cells of $0.05^\circ \times 0.05^\circ$ centered at the nodes of the previous dense grids. In each of the non-overlapping cells, we then estimate, based on at least 50 earthquakes with magnitudes larger than M_c observed till day n after the Chi-Chi shock, the P values in (5) and (8) for $M \geqslant 5.0$ earthquakes that would have occurred during next week (between $n+1$ and $n+7$) days after the Chi-Chi shock. The relative hazard is further computed as the ratio of the individual $\widehat{P}$ value to the maximum of the available $\widehat{P}$ values. Both the RJ and MRJ models, denoted by MRJ-RH and RJ-RH maps, respectively, are finally presented in Fig. 6.

To evaluate how the relative hazard maps perform for identifying the possible rupture regions of $M \geqslant 5.0$ earthquakes in the following week, we construct the Receiver Operating Characteristic (ROC) curves (Swets, 1988) for the MRJ-RH and RJ-RH maps, respectively. In this case, the cells under study with and without $M \geqslant 5$ earthquakes during the following week are denoted by EQ cells and NOEQ cells, respectively. Suppose that such earthquakes are alarmed to occur in the cells with relative hazards greater than a threshold c. Then, the true positive rate (TPR) and false positive rate (FPR) can be computed, accordingly, where the TPR is the probability that earthquakes are successfully alarmed and FPR is the probability for a false alarm as given, respectively, by

$$\mathrm{TPR} = \frac{\text{No. of alarmed EQ cells}}{\text{No. of EQ cells}},$$

and

$$\mathrm{FPR} = \frac{\text{No. of alarmed NOEQ cells}}{\text{No. of NOEQ cells}}.$$

A plot with TPR (y-axis) versus FPR (x-axis) for all possible thresholds then produces the ROC curve. The ROC curves associated with the MRJ-RH and RJ-RH maps, respectively, are also given in Fig. 6. Note that if the RH map is helpful for alarming future earthquakes, then the ROC curve should be above the 45° line. To evaluate the general performance of the two RH maps, we then compute the area under each ROC curve, denoted by AUC. Since the difference between TPR and FPR is the R score (Shi, 2001), we also find the Youden index (Youden, 1950), denoted by J, which is the maximum value of R scores for all possible thresholds. The TPR, FPR, and R score under several different thresholds, along with the AUC and J for each RH map are finally presented in Table 1. In general, the RH map with a larger value of AUC or J is a better alarming system for future earthquakes of interest.

4. Results and discussions

A modified Reasenberg–Jones, or MRJ model is proposed for investigating the temporal and spatial hazard of earthquakes after the Chi-Chi shock. The MRJ model produces, in general, a better sequential forecast for the number of $M \geqslant 5.0$ earthquakes during the next week, as shown in Fig. 5, than does the original RJ model. This is not surprising because, without considering the time effect, the RJ model obtained based on the available earthquakes usually gives a smaller b value than does the MRJ model. Therefore, by using the original RJ model, the earthquake hazard in magnitude enhanced and hence the number of future earthquakes of large magnitude is seriously over-forecasted.

Table 1
Summary statistics for alarming $M \geqslant 5.0$ earthquakes in a 7-day period after the Chi-Chi shock based on relative hazard maps.

Threshold of relative hazard		RJ-RH map				MRJ-RH map			
		5–11	6–12	7–13	8–14	5–11	6–12	7–13	8–14
0.4	TPR	0.89	0.86	0.83	1.00	0.78	0.71	0.83	1.00
	FPR	0.73	0.74	0.78	0.75	0.51	0.49	0.49	0.52
	R score	0.16	0.12	0.05	0.25	0.27	0.22	0.34	0.48
0.5	TPR	0.78	0.86	0.83	1.00	0.78	0.71	0.33	1.00
	FPR	0.68	0.69	0.72	0.64	0.38	0.37	0.38	0.43
	R score	0.10	0.17	0.11	0.36	0.40	0.34	−0.05	0.57
0.6	TPR	0.78	0.71	0.83	0.75	0.56	0.71	0.33	0.75
	FPR	0.60	0.59	0.63	0.54	0.26	0.29	0.29	0.35
	R score	0.18	0.12	0.20	0.21	0.30	0.42	0.04	0.40
0.7	TPR	0.78	0.71	0.83	0.75	0.44	0.57	0.33	0.75
	FPR	0.53	0.53	0.53	0.47	0.16	0.18	0.22	0.24
	R score	0.25	0.18	0.30	0.28	0.28	0.39	0.11	0.51
0.8	TPR	0.67	0.71	0.67	0.75	0.33	0.43	0.17	0.75
	FPR	0.46	0.47	0.43	0.40	0.10	0.11	0.10	0.14
	R score	0.21	0.24	0.24	0.35	0.23	0.32	0.07	0.61
ROC	AUC	0.66	0.66	0.57	0.72	0.69	0.70	0.60	0.85
	J	0.30	0.35	0.32	0.51	0.39	0.48	0.34	0.62

The relative hazard map constructed based on the MRJ model is generally more capable of depicting the possible rupture area of $M \geqslant 5.0$ earthquakes in the following week than the related RJ-RH model. As shown in Fig. 6, the ROC curve corresponding to the MRJ-RH map is higher than the one of the RJ-RH map for alarming earthquakes under study. For example, as indicated in Table 1, both the RJ-RH and MRJ-RH maps with threshold 0.6 successfully alarms 71% of the $M \geqslant 5.0$ earthquakes that occurred during the 6–12 days after the Chi-Chi shock. However, the RJ-RH map issues 58% of gridpoints under study for alarming $M \geqslant 5.0$ earthquakes over the next week, while the alarming area for such earthquakes given by the MRJ-RH map contains only 30% of the gridpoints under study. This is the reason why the MRJ-RH map, which has a smaller alarming area compared to the RJ-RH map, has a much smaller chance of issuing false alarms for next-week earthquakes, although it may not have a larger probability to correctly pinpoint such earthquakes. Hence, the R scores of the MRJ-RH map for the thresholds under study are larger than those of the RJ-RH map. In addition, both the AUC and J of the ROC curve corresponding to the MRJ-RH map are larger than those corresponding to the RJ-RH map. Therefore, the MRJ model is superior to the RJ model for exploring the spatial hazard of $M \geqslant 5.0$ earthquakes during the week after the Chi-Chi shock.

Note that the work on rock mechanics (Scholtz, 1968) infers that regions with low b value correspond to regions of high stress. It has also been found that a lower b value is related to the asperity zone in which the shear stress is higher than its neighboring zones (Wiemer and Wyss, 1997; Sylvander, 1999). In fact, the time-dependent stress transfer might occur in the study region after a drastic earthquake (Toda and Stein, 2003) and thereby produce a variety of b values in space over time. The stress evolution following the 1999 Chi-Chi shock studied by Chan and Stein (2009) further indicates that Coulomb stress increase might promote future $M \geqslant 4.0$ earthquakes. Therefore, when the detailed and accurate information on the stress transfer or stress change is not available in a short time after a drastic shock, a modification the RJ model with the time-varying b values proposed in this paper would be of great help for a real-time forecast of the occurrence of future earthquakes.

Acknowledgements

This study was partially supported by grant MOST 103-2628-M-008-001 from the Ministry of Science and Technology (MOST) to National Central University. The authors wish to thank Dr. Loren Chang for his pre-reading of the manuscript.

References

Aki, K., 1965. Maximum likelihood estimate of b in the formula log N=a-bM and its confidence limits. Bull. Earthquake Res. Inst. 43, 237–239.
Chan, C.H., Stein, R.S., 2009. Stress evolution following the 1999 Chi-Chi, Taiwan, earthquake: consequences for afterslip, relaxation, aftershocks and departures from Omori decay. Geophys. J. Int. 177, 179–192.
Gutenberg, R., Richter, C.F., 1944. Frequency of earthquakes in California. Bull. Seismol. Soc. Am. 34, 185–188.
Kisslinger, C., Jones, L.M., 1991. Properties of aftershocks in southern California. J. Geophys. Res. 96, 11947–11958.
Ogata, Y., 1983. Estimation of the parameters in the modified Omori formula for aftershock sequences by the maximum likelihood procedure. J. Phys. Earth 31, 115–124.
Reasenberg, P.A., Jones, L.M., 1989. Earthquake hazard after a mainshock in California. Science 243, 1173–1176.
Reasenberg, P.A., Jones, L.M., 1994. Earthquake aftershocks: update. Science 265, 1251–1252.
Scholz, C.H., 1968. The frequency-magnitude relation of micro fracturing in rock and its relation to earthquakes. Bull. Seismol. Soc. Am. 58, 399–415.
Shi, Y., Bolt, B.A., 1982. The standard error of the magnitude-frequency b value. Bull. Seismol. Soc. Am. 72, 1677–1687.
Shi, Y., Liu, J., Zhang, G., 2001. An evaluation of Chinese annual earthquake predictions. J. Appl. Probability 38A, 222–231.
Smith, W.D., 1981. The b-value as an earthquake precursor. Nature 289, 136–139.
Swets, J., 1988. Measuring the accuracy of diagnostic systems. Science 240, 1285–1293.
Sylvander, M., 1999. Identifying an asperity through 3-D mapping of the frequency-magnitude distribution. Geophys. Res. Lett. 26, 2657–2660.
Toda, S., Stein, R., 2003. Toggling of seismicity by the 1997 Kagoshima earthquake couplet: a demonstration of time-dependent stress transfer. J. Geophys. Res. 108, 2567. http://dx.doi.org/10.1029/2003JB002527.
Utsu, T., 1971. Aftershock and earthquake statistic (III): analyses of the distribution of earthquakes in magnitude, time and space with special consideration to clustering characteristics of earthquake occurrence (1). J. Fac. Sci., Hokkaido Univ., Ser. VII, Geophys. 3, 379–441.
Utsu, T., Ogata, Y., Matsu'ura, R.S., 1995. The centenary of the Omori formula for a decay law of aftershock activity. J. Phys. Earth 30, 521–605.
Vere-Jones, D., 1992. Statistical methods for the description and display of earthquake catalogs. In: Walden, A.T., Guttorp, P., Arnolde, E. (Eds.), Statistics in the Environmental and Earth Sciences. Wiley, New York.
Wiemer, S., 2000. Introducing probabilistic aftershock hazard mapping. Geophys. Res. Lett. 27, 3405–3408.
Wiemer, S., Gerstenberger, M., Hauksson, E., 2002. Properties of the aftershock sequence of the 1999 M_W7.1 Hector Mine earthquake: implications for aftershock hazard. Bull. Seismol. Soc. Am. 92, 1227–1240.
Wiemer, S., Katsumata, K., 1999. Spatial variability of seismicity parameters in aftershock zones. J. Geophys. Res. 103, 13135–13151.
Wiemer, S., Wyss, M., 1997. Mapping the frequency-magnitude distribution in asperities: an improved technique to calculate recurrence times? J. Geophys. Res. 102, 15115–15128.
Wiemer, S., Wyss, M., 2000. Minimum magnitude of completeness in earthquake catalogs: examples from Alaska, the western US and Japan. Bull. Seismol. Soc. Am. 90, 859–869.
Youden, W.J., 1950. Index for rating diagnostic tests. Cancer 3, 32–35.